ACS Chemical Neuroscience pubs.acs.org/acschemicalneuroscience

Amyloid β-Protein Aggregation Produces Highly Reproducible Kinetic Data and Occurs by a Two-Phase Process

Erik Hellstrand,[‡] Barry Boland,[§] Dominic M. Walsh,[§] and Sara Linse*,[‡]

[‡]Chemistry Department and Molecular Protein Science, Lund University, P.O. Box 124, SE221 00 Lund, Sweden, and
[§]Laboratory for Neurodegenerative Research, Conway Institute, Belfield, University College Dublin, Dublin 4, Republic of Ireland

Abstract

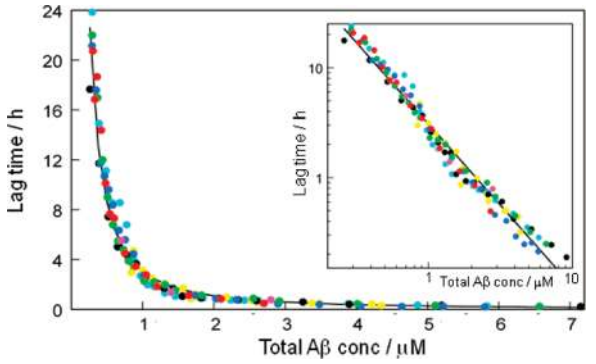

Protein aggregation can lead to major disturbances of cellular processes and is associated with several diseases. We report kinetic and equilibrium data by ThT fluorescence and enzyme-linked immunosorbent assay of sufficient quality and reproducibility to form a basis for mechanistic understanding of amyloid β-peptide (Aβ) fibril formation. Starting from monomeric peptide in a pure buffer system without cosolvents, we find that the kinetics of Aβ aggregation vary strongly with peptide concentration in a highly predictable manner. The free Aβ concentration in equilibrium with fibrils was found to vary with total peptide concentration in a manner expected for a two-phase system. The free versus total Aβ concentration was linear up to ca. 0.2 μM, after which free Aβ decreased with total Aβ toward an asymptotic value. Our results imply that Aβ fibril formation arises from a sequence of events in a highly predictable manner.

Keywords: Amyloid, aggregation, kinetics, mechanism, Alzheimer, fibril

The amyloid β-protein (Aβ) is a ~4 kDa amphipathic polypeptide prone to self-association and fibril formation and is believed to play a causal role in Alzheimer's disease (*1*). Aβ toxicity appears to require self-association and aggregation, but as yet the assembly form(s) of Aβ that mediate disease remain unknown (*2*).

Monomeric Aβ is more or less unstructured in solution (*3*), whereas the fibrillar form has a characteristic cross-β structure with stacking of β strands perpendicular to the long axis of the fiber (*4*−*6*). Accumulated data from many studies suggest that the process leading from monomeric to fibrillar state involves a number of intermediate oligomeric states of different association numbers and structures (*7*, *8*). Kinetic aggregation data have a sigmoidal appearance characteristic of nucleation-dependent polymerization. The process starts with a lag phase, after which elongation into mature fibrils rapidly proceeds. Nonetheless, the molecular mechanism leading from monomer to fibril are poorly understood, and fibril formation is often said to be a stochastic process with large variation in nucleation rate among identical macroscopic samples. This view is in part due to an apparent low reproducibility of kinetic data (*9*). Opposing findings are often based on very few replicates, and systematic studies of the role of physicochemical properties of Aβ and its environment have been hampered by the high costs of synthetic Aβ. We have overcome these obstacles by identification and elimination of factors leading to irreproducibility of the kinetic experiment and by developing a recombinant expression system for production of large quantities of highly pure Aβ (*10*), thus enabling detailed studies using multiple replicates.

Here we have studied the concentration dependence of Aβ(M1−42) aggregation kinetics by means of thioflavin T (ThT) fluorescence and equilibrium by enzyme-linked immunosorbent assay (ELISA). The present work is an attempt to significantly improve the quality of these kinetic and equilibrium assays to approach a mechanistic understanding. While the process *in vivo* occurs in a complex environment with high concentrations of many different proteins, salts, metabolites, and biological membranes, one route toward a mechanistic understanding is systematic investigations of the process in a pure buffer system followed by stepwise introduction of biologically relevant components. The availability of large amounts of highly pure recombinantly expressed peptide and optimization of the experimental aggregation protocols have allowed us to accumulate kinetic and equilibrium

Received Date: September 8, 2009
Accepted Date: October 1, 2009
Published on Web Date: October 09, 2009

DOI: 10.1021/cn900015v | *ACS Chem. Neurosci.* (2010), *1*, 13–18

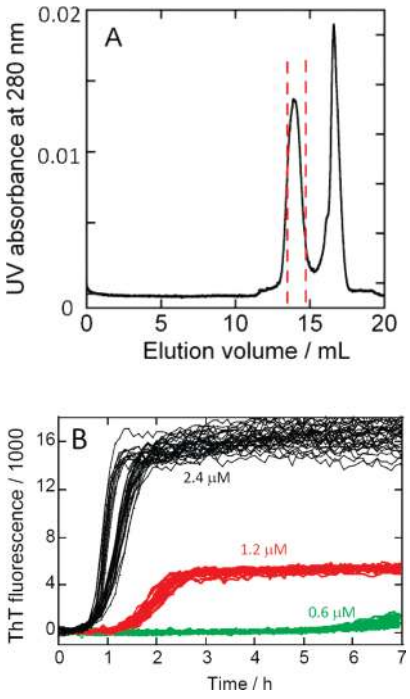

Figure 1. (A) Isolation of monomeric Aβ(M1−42) by gel filtration on a Superdex 75 column in 20 mM sodium phosphate buffer, pH 8, with 200 μM EDTA and 0.02% NaN_3. The monomer is collected between the dashed red lines and is free from higher Aβ assembly forms (shoulder before monomer peak) and buffer and salts (tall peak after the monomer peak). (B) Kinetic traces by ThT fluorescence for 32 replicates at concentrations 2.4 (black), 1.2 (red), and 0.6 μM (green) Aβ(M1−42) in 20 mM sodium phosphate, pH 8, 200 μM EDTA, 0.02% NaN_3, 20 μM ThT. The first 7 h are shown.

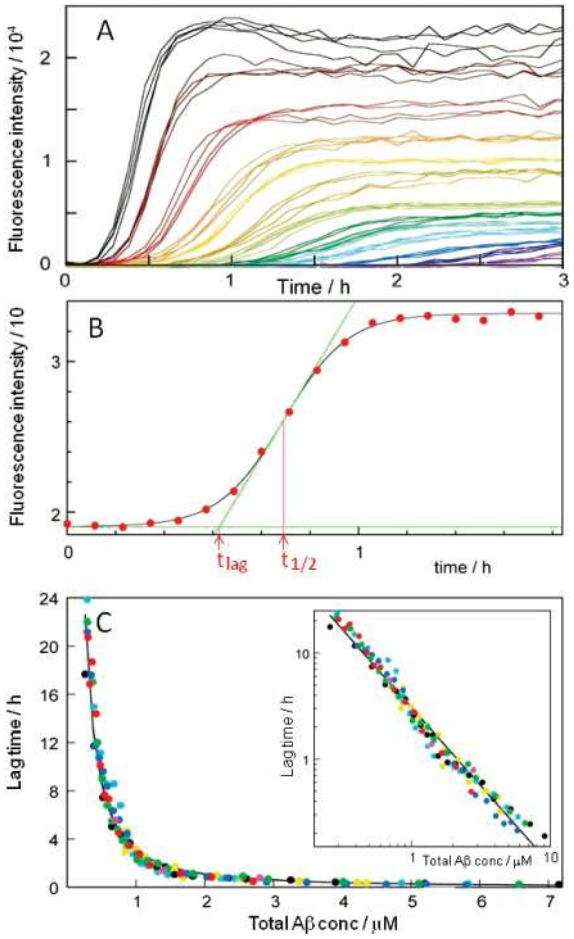

Figure 2. Concentration dependence of Aβ aggregation kinetics in 20 mM sodium phosphate, pH 8, 200 μM EDTA, 0.02% NaN_3, 20 μM ThT. (A) Kinetics of aggregation monitored using ThT fluorescence. Data for the 13 highest concentrations in a single experiment are shown with Aβ(M1−42) concentrations of 5.8 (black), 4.9 (brown), 3.9 (red), 2.9 (orange), 2.6 (yellow), 2.2 (green-yellow), 1.85 (yellow-green), 1.65 (green), 1.46 (cyan), 1.31 (light blue), 1.17 (blue), 1.07 (marine blue), and 0.97 (purple) μM. (B) Fitting of eq 1 to one of the fibrillation traces in panel A, with data points as filled circles and the fitted curve as a solid line. The values for $t_{1/2}$ as obtained by the fit and t_{lag} by eq 2 are indicated. (C) Lagtime obtained by fitting eq 1 to 672 kinetic traces in seven sets of data (in black, red, green, magenta, cyan, yellow, and blue) versus Aβ(M1−42) concentration. Each point is average of 3−32 replicates of the same solution. The solid line is a power function with exponent −1.48 fitted to all data points. Inset: same data with logarithmic axes.

data of sufficient quality and reproducibility to form a basis for mechanistic understanding of Aβ fibrillation.

The aggregation kinetics were studied by means of ThT fluorescence at 100 rpm orbital shaking, and examples of data are shown in Figures 1B and 2A. We observe a high level of reproducibility between replicates of the same solution as regards lag time, elongation rate, and the plateau value of ThT fluorescence after equilibrium is gained, see Figure 1B (32 replicates of each solution) and Figure 2A (4 replicates of each solution). Identified factors that lead to a high reproducibility between replicates of a solution and between experiments set up on different dates are (i) complete degassing and filtering of the buffer used to prepare the samples, (ii) gel filtration of Aβ(M1−42) in the degassed experimental buffer and collection of the monomer on ice just prior to starting the experiment (Figure 1A), (iii) careful pipetting on ice to produce the dilution series without introducing air bubbles, (iv) minimized air−water interface area relative to sample volume (100 μL per well in "half-area" 96-well plates), (v) PEG-coated polystyrene plates, and (vi) absence of any cosolvents or substances other than Aβ and the components of the buffer chosen for the study. Points i−iv are intended to control the amount of accumulation of the surface-active Aβ peptide at the air−water interface by minimizing the surface area of such interfaces. Point v is intended to minimize Aβ binding to the plastic surface of the wells and point vi to avoid disturbances from the cosolvents, including indirect effects on the surface tension of the solvent. Point ii ensures a homogeneous monomeric starting material. In addition, the availability of large amounts of highly pure peptide makes it possible to include sufficient replicates to draw statistically significant conclusions.

DOI: 10.1021/cn900015v | ACS Chem. Neurosci. (2010), 1, 13–18

The lag time, t_{lag}, and the time at half completion of the aggregation process, $t_{1/2}$, were estimated by fitting a sigmoidal function (eq 1) to each kinetic trace, as exemplified in Figure 2B.

$$F(t) = F_0 + A/(1 + \exp(-k(t - t_{1/2}))) \quad (1)$$

The fitted parameters are $t_{1/2}$, the elongation rate constant, k, the amplitude, A, and the baseline before aggregation, F_0. We define the lag time, t_{lag}, as the intercept between the time axis and the tangent with slope k from the midpoint of the fitted sigmoidal curve (Figure 2B). By this definition, t_{lag} was calculated from the fitted parameters as

$$t_{lag} = t_{1/2} - 2/k \quad (2)$$

The lag times from 672 kinetic experiments (in seven 96-well plates with 3, 4, 6, or 32 replicates of each solution) are plotted versus total Aβ(M1−42) concentration in Figure 2C (linear scale plot) and Figure 2C, inset (log−log plot). Clearly, the lag time is strongly dependent on the total Aβ concentration, that is, on the monomer concentration at the start of each kinetic experiment. Moreover, data recorded on seven different days superimpose within error limits (separate colors in Figure 2C). The kinetics of amyloid β peptide (Aβ) aggregation thus vary strongly with peptide concentration in a highly predictable manner.

The simplest function that fits reasonably well to the lag time versus total Aβ concentration is a power function (eq 3).

$$t_{lag}(c) = Bc^{\alpha} \quad (3)$$

where c is the Aβ concentration, B is a proportionality constant, and α is the exponent. Optimal fit is obtained with $B = 1.5 \times 10^{-5}$ h and $\alpha = -1.5$. If instead the half times, $t_{1/2}$, from the 672 kinetic experiments are plotted versus total Aβ(M1−42), the overall appearance of the plot is very similar (not shown). The optimal fit of eq 4 to the $t_{1/2}$ data is obtained with $D = 2.3 \times 10^{-5}$ h and $\beta = -1.5$, and the magnitude of the deviation of the points from the fitted curve is the same as in Figure 2C.

$$t_{1/2}(c) = Dc^{\beta} \quad (4)$$

The exponent of −1.5 is in line with the steep concentration dependence of the lag time (and of $t_{1/2}$). This is an intriguing finding because an exponent of −1.5 also describes the concentration dependence of diffusion-controlled bimolecular collisions; however, the length of the lag phase suggests that only a fraction of the encounters are productive. The close correspondence of the data with a power function with exponent of −1.5 suggests that the nucleation of Aβ fibril formation is dependent on simple physical principles. For a nucleated polymerization reaction with of size n, in the absence of secondary processes, the concentration dependence of the polymerization rate will follow a power function with exponent $(n + 1)/2$; thus the exponent of −1.5 suggests a nucleus of size two (*11*).

Similar data for concentration dependence of β2-microglobulin (β2m) fibrillation have been fitted using a power function with exponent −0.81, roughly half of what we find here for Aβ(M1−42) (*12*). This suggests that while secondary processes, for example, fibril breakage contribute to the lag time of β2m fibril formation (*11*, *12*), the concentration dependence of the Aβ lag time is to a larger extent governed by the primary nucleation event.

The kinetic data reported here is of sufficient quality and reproducibility to form a basis for mechanistic understanding of amyloid β peptide (Aβ) fibrillation. The precision of the data is in bright contrast to earlier reports showing a spread in t_{lag} from 7 to 19 h between apparently identical samples of 2.2 μM His_6-Aβ(1−40), which was interpreted to imply that nucleation is under the influence of a stochastic factor that manifests itself in macroscopic differences in the aggregation kinetics (*9*). Each kinetic trace reported here is obtained for 2×10^{13} to 8×10^{14} molecules (100 μL of 0.26−12 μM Aβ), a number that would make stochastic behavior unlikely.

Aβ is reported to have a critical concentration below which fibrils cannot form (*13*). Here we observe ThT-positive aggregates at Aβ concentrations of 0.26 μM or higher. Below 0.26 μM, the expected fluorescence increase due to aggregation is below the noise level. Therefore, below 0.26 μM, it is impossible to assess whether aggregates will eventually form or not. To assess the aggregation at lower concentrations, the concentration of Aβ remaining in solution in equilibrium with aggregates was quantified after centrifugation using a sensitive ELISA (Figure 3). This ELISA predominantly detects Aβ monomer but not Aβ assemblies (*14*, *15*).

The equilibrium data display an initial linear rise in free Aβ up to ca. 0.2 μM total Aβ. A slope close to 1 (the slope of 0.81 reflects the mode of standardization of the ELISA) and the strong linearity in this regime implies that free Aβ is equal to total Aβ and no fibrils (or an insignificant amount of fibrils) are formed. There are two possible interpretations of this behavior. Either there is a critical concentration below which fibrils cannot form (*13*), or a concentration of 0.2 μM is needed for aggregates to form during the time frame of the experiment (up to one week) in enough quantities that the difference between free and total Aβ will be larger than the experimental error of the ELISA.

Above 0.2 μM, free Aβ decreases as total Aβ increases, opposite to what one would expect for association equilibria in solution. Our data are thus indicative of aggregation and phase separation in this

DOI: 10.1021/cn900015v | ACS Chem. Neurosci. (2010), 1, 13–18

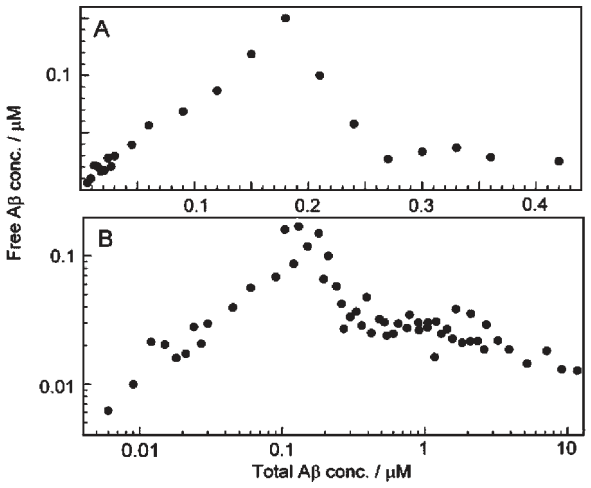

Figure 3. Concentration dependence of Aβ aggregation equilibrium in 20 mM sodium phosphate, pH 8, 200 μM EDTA, 0.02% NaN_3. Samples were allowed to aggregate for 84−96 h, and large aggregates were removed by centrifugation. The concentration of soluble Aβ determined by ELISA is plotted versus total concentration (from acid hydrolysis): (A) low concentration samples, linear axes; (B) all samples, logarithmic axes.

concentration regime. The behavior above 0.2 μM suggests a two-phase region where one of the phases is in such small amount that surface effects contribute significantly to its chemical potential. The two phases are soluble Aβ (liquid phase) and Aβ aggregate (solid phase). After the linear rise, we observe an initially steep negative trend in free versus total Aβ (between ca. 0.2 and 0.3 μM total Aβ) followed by a shallow negative trend asymptotically approaching a limiting value. We cannot exclude the possibility that some sample(s) around 0.2 μM are yet not in equilibrium. Nevertheless, the observed behavior above 0.2 μM suggests that the average chemical potential of the peptide in small aggregates is just barely lower than that of free Aβ at low concentration, most likely because in small aggregates the fraction of peptides at the ends or surfaces of the aggregate is significant. The average chemical potential of the peptide in aggregates becomes lower and lower as aggregates grow and the number of peptides at ends becomes a smaller and smaller fraction. The asymptotic behavior at high total Aβ implies that the chemical potential in the aggregate reaches a limiting value, because the fraction of peptides at ends of aggregates become insignificant, or the fibril length reaches a limiting value. This interpretation relies on the fact that amyloid fibrils increase in size with increased total protein concentration, as found from Aβ simulations (*16*) and experimentally for α-synuclein (*17*).

Our results imply that the nucleation-dependent polymerization of Aβ is not stochastic on a macroscopic level but arises from a sequence of events in a predictable manner. Our data agree with a critical concentration around 0.2 μM Aβ(M1−42) in 20 mM sodium phosphate, pH 8, 200 μM ethylenediaminetetraacetic acid (EDTA), and 0.02% NaN_3 below which aggregates cannot be detected. This limit is lower than 0.7−1.0 μM obtained for Aβ(1−40) in phosphate-buffered saline (*13*), likely due to differences in peptide length and ionic strength.

The experimental precision reported here will make it possible to gain greater insights into the molecular mechanism of Aβ fibrillation and to better study conditions and agents that influence aggregation (*5*, *18*, *19*). The presented results imply that Aβ fibrillation proceeds by a sequence of reactions in a highly predictable manner and offer a useful model to test and develop inhibitors of various stages of Aβ aggregation.

Methods

Materials

All chemicals were of analytical grade. The Aβ(M1−42) peptide (MDAEFRHDSGYEVHHQKLVFFAEDVGSNKGAIIGLMVGGVVIA) was expressed in *Escherichia coli* and purified as described previously (*10*). In short, the purification procedure involved sonication of *E. coli* cells, dissolution of inclusion bodies in 8 M urea, ion exchange in batch mode on DEAE cellulose resin, centrifugation through a 30 kDa molecular weight cutoff (MWCO) filter, and finally concentration using a 3 kDa MWCO filter. The purified peptide was frozen as identical 1 mL aliquots.

Preparation of Samples for Kinetic Experiments

For kinetic experiments, aliquots of purified Aβ(M1-42) were thawed and subjected to gel filtration on a Superdex 75 column in 20 mM sodium phosphate buffer, pH 8, with 200 μM EDTA and 0.02% NaN_3. The latter part of the monomer peak (Figure 1A) was collected on ice and was typically found to have a concentration (determined by quantitative amino acid analysis; this analysis was purchased from BMC Uppsala) of 5−12 μM.

The gel filtration step removes traces of pre-existent aggregates and exchanges the buffer to that required for the fibrillation experiment. The collected monomer was supplemented with 20 μM thioflavin T (ThT) from a 2 mM stock and was used to prepare dilution series between 0.01 and 12 μM Aβ(M1−42) in 20 mM sodium phosphate buffer, pH 8, with 200 μM EDTA and 0.02% NaN_3, which was also supplemented with 20 μM ThT before producing the dilution series so that all samples contain the same ThT concentration. The dilutions were made in tubes on ice using careful pipetting to avoid introduction of air bubbles. Each sample was then pipetted into multiple wells of a 96 well half-area plate of black polystyrene with clear bottom and PEG coating (Corning 3881), 100 μL per well. The circular bottom of the wells in "half-area" plates have half the area of wells in regular 96 well plates. The samples were added to the plate from lower to higher concentration after which the plate was sealed with a plastic film (Corning 3095).

Kinetic Aggregation Experiment

The experiment was initiated by placing the 96-well plate at 37 °C and shaking at 100 rpm in a plate reader (Fluostar Omega,

DOI: 10.1021/cn900015v | *ACS Chem. Neurosci.* (2010), *1*, 13–18

BMG Labtech, Offenburg, Germany). The ThT fluorescence was measured through the bottom of the plate every 6 min (with excitation filter 440 nm and emission filter 480 nm) with continuous shaking at 100 rpm between reads. The ThT fluorescence was followed for seven different 96-well plates (two plates with 32 samples in triplicate, three plates with 24 samples in quadruplicate, one with 16 samples in hexaplicate, and one with 3 samples in 32 replicates) yielding in total 672 kinetic traces.

ELISA (Enzyme-Linked Immunosorbent Assay)

The free Aβ(M1−42) concentration at equilibrium over fibrils was analyzed by ELISA as follows for samples set up in parallel to those described above but without ThT in the solution, with shaking at 100 rpm for up to 1 week. This procedure mainly quantifies the monomeric Aβ (*14*, *15*). Supernatants over fibrils were collected after centrifugation at 13 000*g* for 10 min and diluted 1:100 in EC buffer (20 mM sodium phosphate, 2 mM EDTA, 400 mM NaCl, 0.2% bovine serum albumin (BSA), 0.05% 3-[(3-cholamidopropyl)dimethylammonio]-1-propanesulfonate (CHAPS), 0.4% Block Ace (Dainippon Pharmaceutical Co., Osaka, Japan), 0.05% NaN_3, pH 7.0). The standard series was diluted from a stock prepared from synthetic Aβ(1−42) peptide (American Peptide, Sunnyvale, CA) in 0.1% NH_4OH. The concentration of this stock was based on optical density absorbance of peptide solution at 275 nm. The ELISA was performed in Nunc-Immuno Plate (MaxiSorp surface, Nunc A/S, Roskilde, Denmark). Capture antibody (C-terminal specific antibody for Aβ42, JRF/cAb42/26, from Centocor, Horsham, PA) was used at 2.5 μg/mL in 30 mM $NaHCO_3$, 70 mM Na_2CO_3, 0.05% NaN_3, pH 9.6, and 100 uL was added to each well and incubated overnight at 4 °C with rocking. The solution was removed, and wells were washed twice with PBS (6 mM sodium phosphate, 137 mM NaCl, 3 mM KCl, pH 7.4) followed by addition of 200 μL blocking solution (1% Block Ace, 0.05% NaN_3, PBS, pH 7.4) to each well. The plates were incubated for 4 h at room temperature with rocking. The blocking solution was removed by dumping, followed by immediate addition of 50 μL of EC buffer to each well to prevent the wells from drying while adding samples. To each well, 100 μL of sample, standard, or blank was added, and plates were incubated overnight at 4 °C with rocking. The wells were washed twice with PBST (PBS with 0.05% Tween 20) and once with PBS. Horseradish peroxidase (HRP)-conjugated detection antibody (JRF/Abtot/17, diluted 1:2500 from the stock) that recognizes amino acids 1−17 of Aβ(M1−42) from Centocor was diluted in 20 mM sodium phosphate, 2 mM EDTA, 400 mM NaCl, 1% BSA, pH 7.0, and was added to each well (100 μL per well), and the plates incubated for 4 h at room temperature with rocking. Wells were again washed twice with PBST, and once with PBS. Substrate solution (100 μL of TMB 2-Component Microwell Peroxidase Substrate Kit from Kirkegaard and Perry Laboratories, Gaithersburg, MD, cat. no. 50-76-00) was added to each well, and the color reaction was allowed to proceed until the second to the least concentrated standard had a slight color change, when the reaction was stopped by adding 100 μL of 5.8% *o*-phosphoric acid in H_2O to each well. The absorbance at 450 nm was recorded for all wells using a microplate reader (Molecular Devices SpectraMax M2 microplate reader, Sunnyvale, CA).

Author Information

Corresponding Author

*Corresponding author. E-mail: Sara.Linse@biochemsitry.lu.se.

Funding Sources

This work was supported by the Swedish Research Council Linneaus Centre "Organizing Molecular Matter" (SL), Greta och Johan Kock's Foundation (SL), and Wellcome Trust grant 067660 (DMW). BB is a Health Research Board Fellow.

Acknowledgment

We thank Kyrre Thalberg, Lund, for stimulating scientific discussion on phase transition behavior and Dusan Raicevic for directing us to PEG-coated half-area plates.

References

1. Selkoe, D. J. (2001) Alzheimer's disease: Genes, proteins, and therapy. *Physiol. Rev. 81*, 742–761.

2. Walsh, D. M., and Selkoe, D. J. (2007) A beta oligomers-a decade of discovery. *J. Neurochem. 101*, 1172–1184.

3. Walsh, D. M., Hartley, D. M., Kusumoto, Y., Fezoui, Y., Margaret, M., Condron, M. M., Lomakin, A., Benedek, G. B., Selkoe, D. J., and Teplow, D. B. (1999) Amyloid beta-protein fibrillogenesis. Structure and biological activity of protofibrillar intermediates. *J. Biol. Chem. 274*, 25945–25952.

4. Nelson, R., and Eisenberg, D. (2006) Structural models of amyloid-like fibrils. *Adv. Protein Chem. 73*, 235–282.

5. Sato, T., Kienlen-Campard, P., Ahmed, M., Liu, W., Li, H., Elliott, J. I., Aimoto, S., Constantinescu, S. N., Octave, J. N., and Smith, S. O. (2006) Inhibitors of amyloid toxicity based on beta-sheet packing of Abeta40 and Abeta42. *Biochemistry 45*, 5503–5516.

6. Petkova, A. T., Yau, W. M., and Tycko, R. (2006) Experimental constraints on quaternary structure in Alzheimer's beta-amyloid fibrils. *Biochemistry 45*, 498–512.

7. Mastrangelo, I. A., Ahmed, M., Sato, T., Liu, W., Wang, C., Hough, P., and Smith, S. O. (2006) High-resolution atomic force microscopy of soluble Abeta42 oligomers. *J. Mol. Biol. 358*, 106–119.

8. Finder, V. H., and Glockshuber, R. (2007) Amyloid-beta aggregation. *Neurodegener. Dis. 4*, 13–27.

9. Hortschansky, P., Schroeck, V., Christopeit, T., Zandomnebeghi, G., and Fändrich, M. (2005) The aggregation kinetics of Alzheimer's beta-amyloid peptide is controlled by stochastic nucleation. *Protein Sci. 14*, 1753–1759.

10. Walsh, D. M., Thulin, E., Minogue, A., Gustafsson, T., Pang, E., Teplow, D. B., and Linse, S. (2009) A facile method

DOI: 10.1021/cn900015v | *ACS Chem. Neurosci.* (2010), *1*, 13–18

for expression and purification of the Alzheimer disease-associated amyloid β-peptide. *FEBS J. 276*, 1266–1281.

11. Ferrone, F. (1999) Analysis of protein aggregation kinetics. *Methods Enzymol. 309*, 256–274.

12. Xue, W.-F., Homans, S. W., and Radford, S. E. (2008) Systematic analysis of nucleation-dependent polymerization reveals new insights into the mechanism of amyloid self-assembly. *Proc. Natl. Acad. Sci. U.S.A. 105*, 8926–8931.

13. O'Nuallain, B, Shivaprasad, S, Kheterpal, I, and Wetzel, R. (2005) Thermodynamics of A beta(1−40) amyloid fibril elongation. *Biochemistry 44*, 12709–12718.

14. Stenh, C., Englund, H., Lord, A., Johansson, A. S., Almeida, C. G., Gellerfors, P., Greengard, P., Gouras, G. K., Lannfelt, L., and Nilsson, L. N. (2005) Amyloid-beta oligomers are inefficiently measured by enzyme-linked immunosorbent assay. *Ann. Neurol. 58*, 147–150.

15. Enya, M., Morishima-Kawashima, M., Yoshimura, M., Shinkai, Y., Kusui, K., Khan, K., Games, D., Schenk, D., Sugihara, S., Yamaguchi, H., and Ihara, Y. (1999) Appearance of sodium dodecyl sulfate-stable amyloid beta-protein (Abeta) dimer in the cortex during aging. *Am. J. Pathol. 154*, 271–279.

16. van Gestel, J., and de Leeuw, S. W. (2006) A statistical-mechanical theory of fibril formation in dilute protein solutions. *Biophys. J. 90*, 3134–3145.

17. van Raaij, M. E., van Gestel, J., Segers-Nolten, I. M. J., de Leeuw, S. W., and Subramaniam, V. (2008) Concentration dependence of alpha-synuclein fibril length assessed by quantitative atomic force microscopy and statistical-mechanical theory. *Biophys. J. 95*, 4871–4878.

18. Cabaleiro-Lago, C., Quinlan-Pluck, F., Lynch, I., Lindman, S., Minogue, A. M., Thulin, E., Walsh, D. M., Dawson, K. A., and Linse, S. (2008) Inhibition of amyloid beta protein fibrillation by polymeric nanoparticles. *J. Am. Chem. Soc. 130*, 15437–15443.

19. Linse, S, Cabaliero-Lago, C, Xue, W-F, Lynch, I, Lindman, S, Thulin, E, Radford, S. R., and Dawson, K. A. (2007) Nucleation of protein fibrillation by nanoparticles. *Proc. Natl. Acad. Sci. U.S.A. 104*, 8691–8696.

DOI: 10.1021/cn900015v | *ACS Chem. Neurosci.* (2010), *1*, 13–18